Whole Body Diffusion-Weighted MRI for Bone Marrow Tumor Detection

Heminder Sokhi, MBCHB, MRCS, FRCR; Anwar R. Padhani, MB BS, FRCP, FRCR

Paul Strickland Scanner Centre, Mount Vernon Cancer Centre, Northwood, Middlesex, UK

Background

Recent years have seen the evolution of body diffusion-weighted MRI (DWI) into an exciting, whole body (WB-DWI) imaging technique with a distinct clinical utility, particularly in the context of cancer imaging [1-3]. It is clear that, with its excellent sensitivity for detecting marrow infiltration and good spatial resolution, WB-DWI has the capability of providing functional information which complements conventional anatomic MRI methods. At our institution, we use WB-DWI principally for evaluation of bone marrow metastases, both for detection and for evaluating disease response to therapy, where we have found particular utility for multiple myeloma, breast and prostate cancer. The technique is particularly useful when there is a need to minimize radiation exposure for serial evaluation of younger patients, pregnant women with cancer and in those in whom intravenous contrast medium is contraindicated (allergy or impaired renal function). This article focuses on the technique for Siemens systems, common artifacts encountered in clinical practice, and alludes to its clinical utility regarding skeletal metastases detection. We do not discuss response assessment of malignant bone marrow disease in any detail but there are clear strengths in this regard also [2].

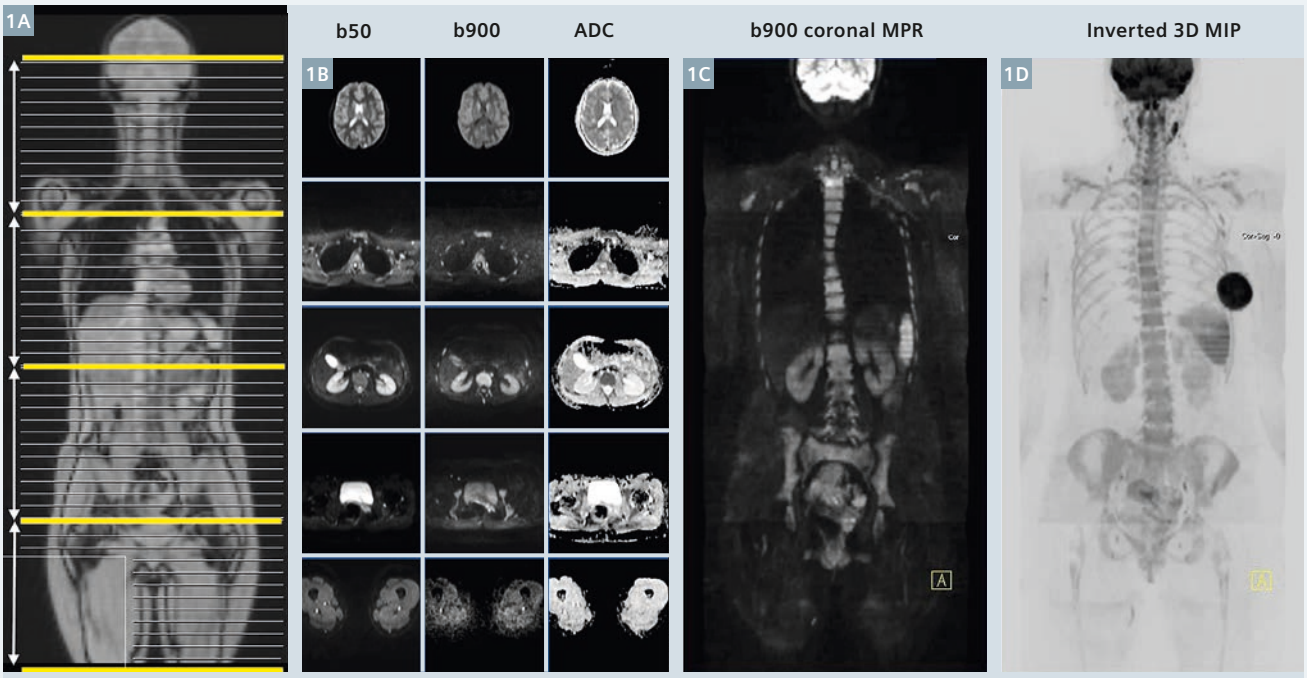

1 **WB-DWI workflow.** 27-year-old woman with sarcomatoid left breast cancer. The bone marrow pattern is normal for age. Axial DWI from the skull base to the mid-thigh is performed using 2 b-values (50 and 900 s/mm²) with a slice thickness of 5 mm in 4 stations. The b900 images are reconstructed into the coronal plane (5 mm) and displayed as thick 3D MIPs (inverted grey scale). ADC images are computed inline with mono-exponential fitting of b50 and b900 signal intensities.

Technique of whole body DWI

Although imaging at 3T increases the signal-to-noise ratio, WB-DWI at this field strength remains challenging because of increased susceptibility artifacts and poorer fat suppression; currently, we find that WB-DWI is best performed on a longer bore 1.5T scanner. All our WB-MRI scans are done on a Siemens MAGNETOM Avanto scanner equipped with a continuous moving table option (TimCT) and total imaging matrix (Tim) body surface coils. We always acquire morphologic images to accompany the WB-DWI images.

Our morphologic images consist of

1. whole spine: T1-weighted, turbo spin-echo sagittal images (acquisition time 2:21 minutes),
2. whole spine: T2-weighted, turbo spin-echo sagittal images with spectral fat suppression (acquisition time 2:36 minutes),
3. whole body: T1-weighted, gradient-echo axial 2-point Dixon sequence (acquisition time 3:00 minutes) that automatically generates four image-sets (in-phase, opposed phase, water-only (WO), and fat-only (FO)) from which T1w fat% and non-fat% images can be calculated if needed.
4. Finally whole body (vertex to upper mid thighs): T2-weighted, short-tau inversion recovery (STIR) axial images with half-Fourier single shot turbo spin-echo (HASTE) readouts (acquisition time 4:00 minutes) is also undertaken.

The axial images from the skull vault to the mid-thighs are acquired using the continuous table movement technology, employing multiple breath-holds for image acquisitions of the chest, abdomen, pelvis and upper thighs.

Axial DWI from the skull vault to the mid-thighs is then performed using b-values of 50 s/mm² and a b-value of 900 s/mm² with a slice thickness of 5 mm. The axial DWI acquisition is usually achieved in 4 contiguous stations using a free-breathing technique, with each station taking approximately 6 minutes to acquire. Our preferred

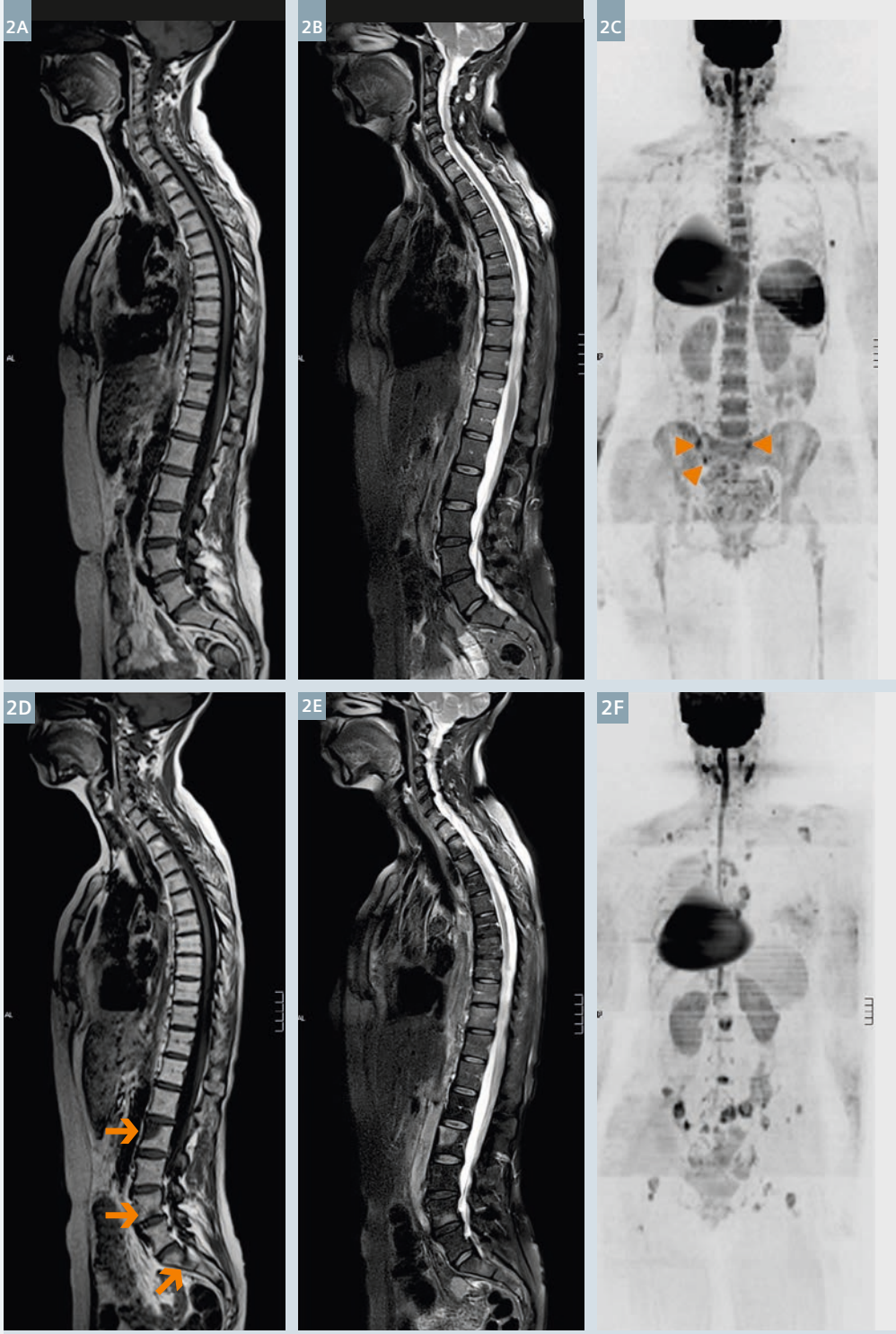

2 **Bone marrow hypoplasia due to chemotherapy with disease progression.**
49-year-old woman with metastatic breast cancer before and after 3 cycles of carboplatin chemotherapy. Both rows left-to-right: spine T1w spin-echo, spine T2w spin-echo with spectral fat saturation and b900 3D MIP (inverted scale) images.
Top row before chemotherapy shows normal background bone marrow pattern with superimposed small volume bone metastases (arrow heads).
Bottom row after chemotherapy shows disease progression with enlarging and new bony metastases (arrows). Note that bone marrow hypoplasia has developed in the ribs, spine and pelvis. Note reductions of signal intensity of the spleen secondary to iron deposition due to blood transfusions. There is a right sided silicone containing breast enhancement bra pad in place on both examinations.

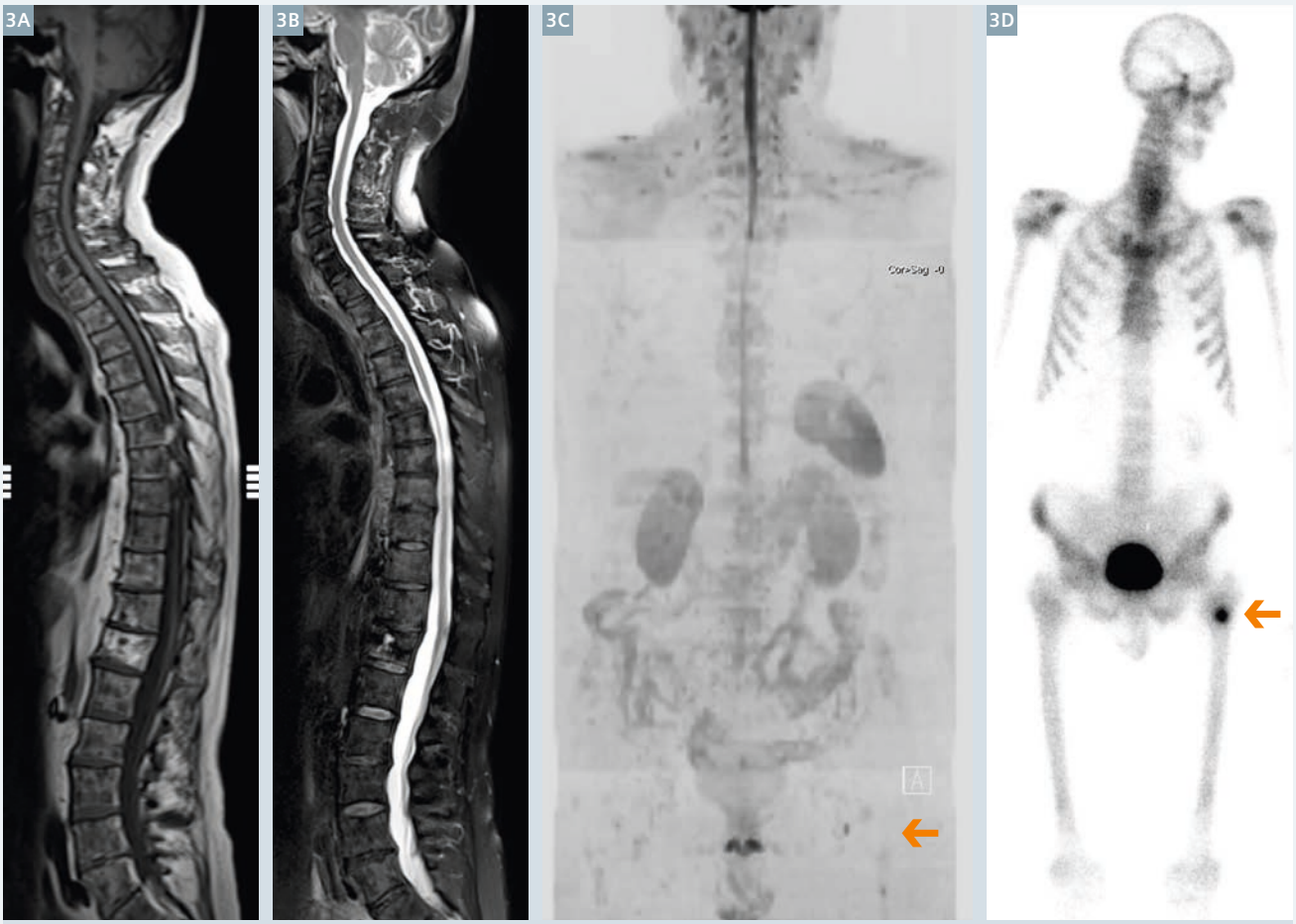

3 **Poor visibility of treated metastases and osteoblastic metastases.** 69-year-old with metastatic prostate cancer on long term, third line hormonal therapy with abiraterone being evaluated for rising serum prostate specific antigen (PSA) levels. He has had an excellent response to 2 years of treatment with residual abnormalities in his bone marrow visible on T1w **(3A)** and T2w (with fat suppression) spinal images. No hyperintensity is seen on the b900 3D MIP (inverted scale) image **(3C)** indicating the absence of highly cellular infiltrative disease. Bone scan **(3D)** shows a focal area of osteoblastic uptake in the intertrochanteric region of the left femur (arrow) which is not visible as a discrete region on the b900 3D inverted MIP image.

method for fat suppression uses inversion recovery because it allows uniform fat suppression over large fields-of-view [4]. An artificially 'fractured spine' observed on the post processed stitched images as a consequence of alignment mismatch can be minimized by manually adjusting and maintaining the transmitter frequency for each station. The b900 value images are reconstructed in the coronal plane (5 mm) and as thick 3D maximum intensity projections (MIPs) which are displayed using an inverted grey scale. ADC maps are computed inline with system software using mono-exponential fitting in which each voxel reflects the tissue diffusivity (units: $\mu m^2/s$) (Fig. 1).

Detailed scanning parameters for each sequence have been published [4, 5]; the entire examination takes 52 minutes to complete. The illustrations of this article were obtained from more than 2,000 WB-DWI scans done at our institution in the last 4 years using this protocol.

Normal bone marrow signal on WB-DWI

A thorough understanding of normal bone marrow signal distribution on b900 value images is vital for the accurate detection, characterization and treatment assessment of skeletal metastases [5]. This is because the bone marrow distribution can be visualized by WB-DWI. The normal adult bone marrow pattern which is established by the age of 25 years can be seen as uniformly distributed, intermediate high signal intensity distributed in the axial skeleton (mixed red bone marrow); yellow marrow in the appendicular skeleton shows no/lower signal intensity (Fig. 1). The changing distribution of the normal marrow is also exquisitely demonstrated on WB-DWI. Red marrow conversion to yellow marrow is dependent on patient age, gender and underlying medical conditions [6]. Both bone marrow hypo- and hypercellularity are well depicted on WB-DWI.

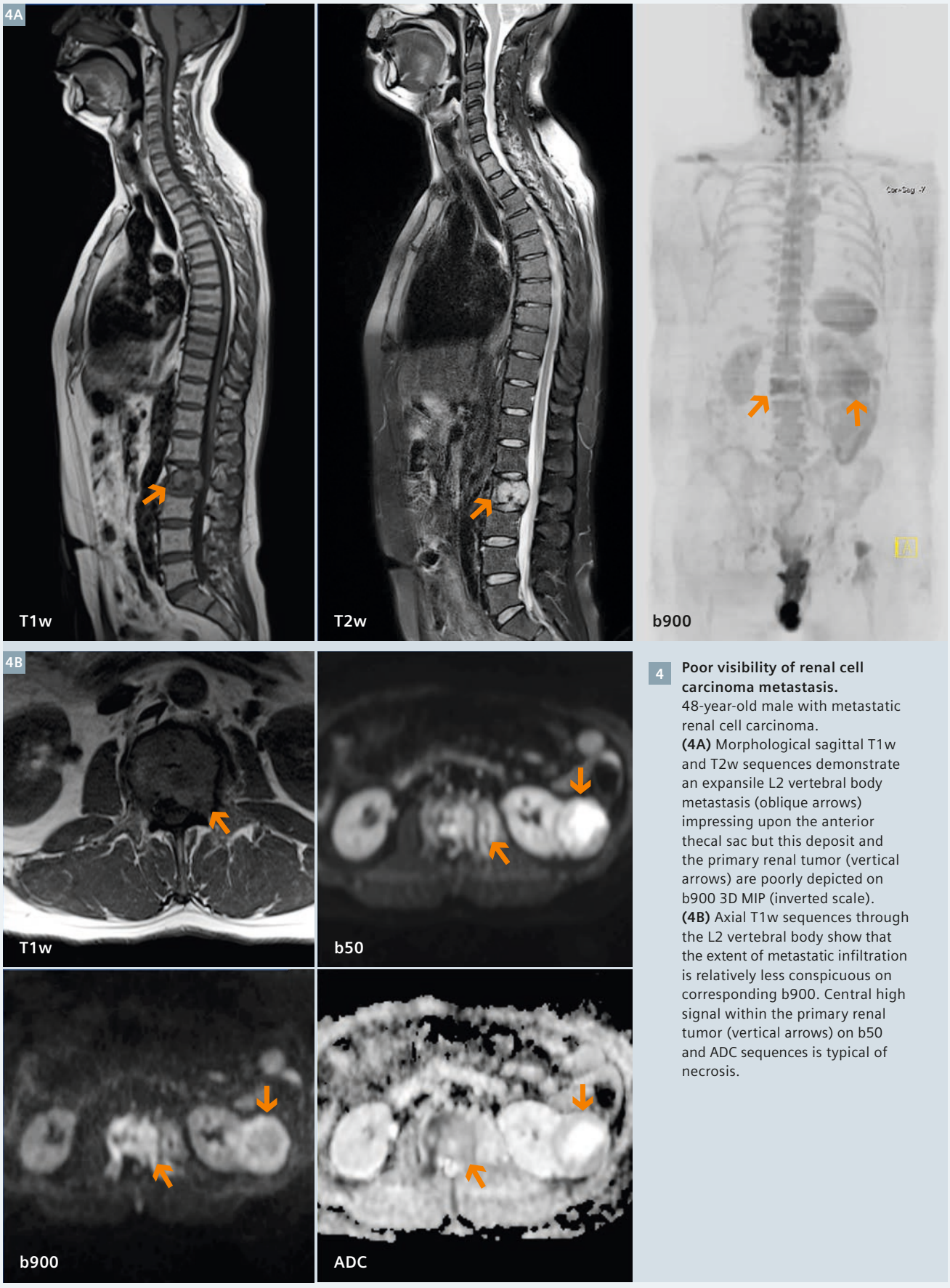

4 Poor visibility of renal cell carcinoma metastasis.
48-year-old male with metastatic renal cell carcinoma.
(4A) Morphological sagittal T1w and T2w sequences demonstrate an expansile L2 vertebral body metastasis (oblique arrows) impressing upon the anterior thecal sac but this deposit and the primary renal tumor (vertical arrows) are poorly depicted on b900 3D MIP (inverted scale).
(4B) Axial T1w sequences through the L2 vertebral body show that the extent of metastatic infiltration is relatively less conspicuous on corresponding b900. Central high signal within the primary renal tumor (vertical arrows) on b50 and ADC sequences is typical of necrosis.

The relationship between bone marrow cellularity and ADC values is non linear and highly dependent on the water, cellular and fat content of the marrow. The reduced water content [6], the larger-sized fat cells, the hydrophobic nature of fat and poorer perfusion all contribute to lower diffusion-weighted signal intensities and ADC values of the yellow bone marrow. On the other hand, with increasing cellularity and water content and greater perfusion, mixed yellow-red bone marrow returns higher signal intensities and paradoxically higher ADC values [5, 7-9].

Skeletal metastases detection

Skeletal metastases appear as focal or diffuse areas of high-signal intensity on high b-value WB-DWI (Fig. 2). The ability to detect bone marrow lesions is dependent on the intrinsic signal intensity of the deposits and the background bone marrow. Other factors determining the visibility of bone lesions include their anatomic location and treatment status. It is imperative that WB-DWI is performed and interpreted in conjunction with conventional morphological WB-MRI sequences rather than in isolation.

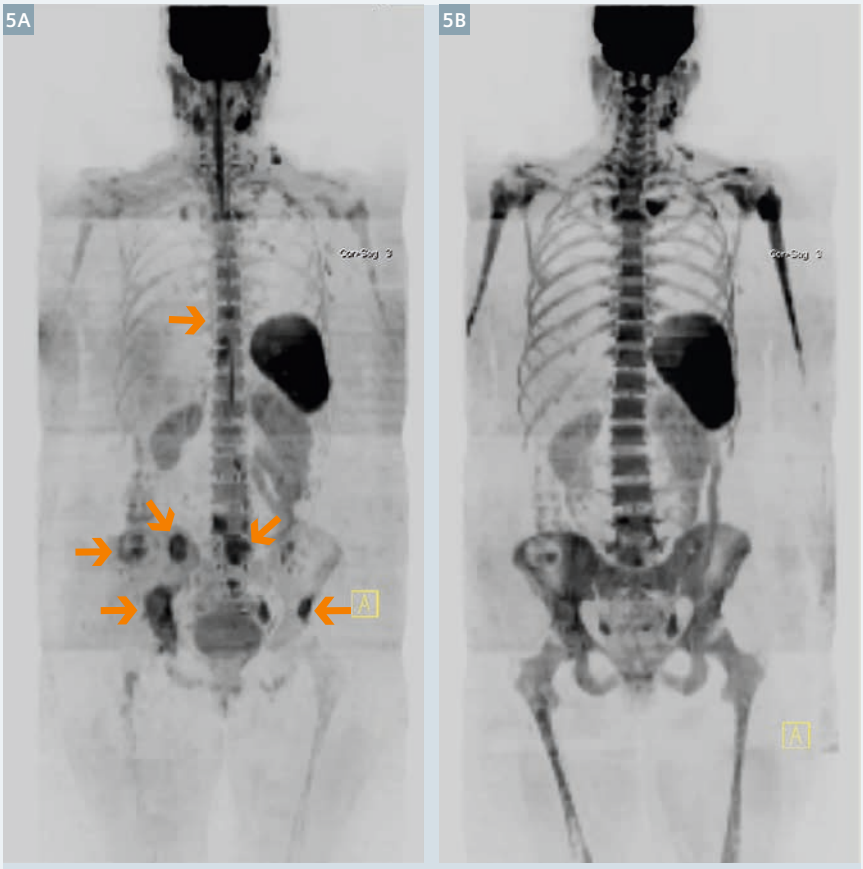

5 **Bone marrow hyperplasia induced by G-CSF therapy obscuring metastases.** 50-year-old woman with metastatic breast cancer before and after 3 cycles of erubulin chemotherapy with growth-colony stimulating factor (G-CSF) given to prevent neutropenia. b900 3D MIP (inverted scale) images. Image 5A shows multiple bone metastases (arrows). Image 5B after 3 cycles of chemotherapy shows increases in signal intensity of the bone marrow leading to the decreased visibility of the bone metastases. The splenic size has also increased. The increased signal intensity of the background bone marrow should not be misinterpreted as malignant progression.

This is because false positive and negative lesions do occur. This assertion was highlighted by a recent meta-analysis, which demonstrated that the high sensitivity of WB-DWI to detect metastases was at the expense of specificity [1].

Generally, infiltrative cellular lesions are better detected than *de-novo* sclerotic or treated lytic/sclerotic lesions (Fig. 3). This is due to the lower water and cellular content of sclerotic and treated metastases [7, 10]. This is the likely reason for the improved visibility of bone metastases of untreated breast cancer compared to prostate cancer; *de-novo* sclerotic metastases are commoner in prostate cancer. WB-DWI is better at detecting skeletal lesions from smaller cancer cell infiltrations such as those due to breast cancer, myeloma, lymphoma and small cell cancers as well as neuroendocrine tumors. On the other hand, bony metastases from clear cell renal cancers are sometimes poorly depicted (the presence of necrosis, large sized tumor cells and inherent lipogenesis contribute to the poorer visualization) (Fig. 4). On occasion, the high magnetic field susceptibility of melanin can also impair depiction of melanoma metastases.

The detection of skeletal metastases on WB-DWI may be impaired in areas of movement such as the anterior ribs and sternum. Visibility of skull vault infiltrations can be impaired because of the adjacent high signal of the normal brain. The visibility of skull base disease is impaired because of susceptibility effects.

Other causes for false-negative findings are low levels of bone marrow infiltration such as in smoldering multiple myeloma (when plasma cell infiltration fraction is less than background cell bone marrow cellularity) or when bone marrow hyperplasia results in diffuse increase in signal on high b-value images obscures the presence of metastases [2, 5] (Fig. 5). Relative bone marrow hypercellularity is observed in children and adolescents, chronic anemia, in smokers, chronic cardiac failure, in pregnancy

6 False positive whole body diffusion MRI.
64-year-old female with breast cancer treated with right mastectomy, radiotherapy and chemotherapy. **(6A)** Bone scan shows increased uptake at L4/L5 – query metastases. **(6B)** Subsequent WB-DWI imaging 1 month later shows normal signal at L4/L5 with normal anatomic MRI images, but reveals a small focus of high signal intensity overlying the sacrum on b900 3D MIP (vertical arrow) and axial images. Corresponding anatomical T1w and STIR sequences show no focal abnormality within the sacrum; the high signal seen on b900 images is artifact from adjacent bowel. Note normal marrow signal on WB-DWI done eight months later (bottom right) with no development of metastases.

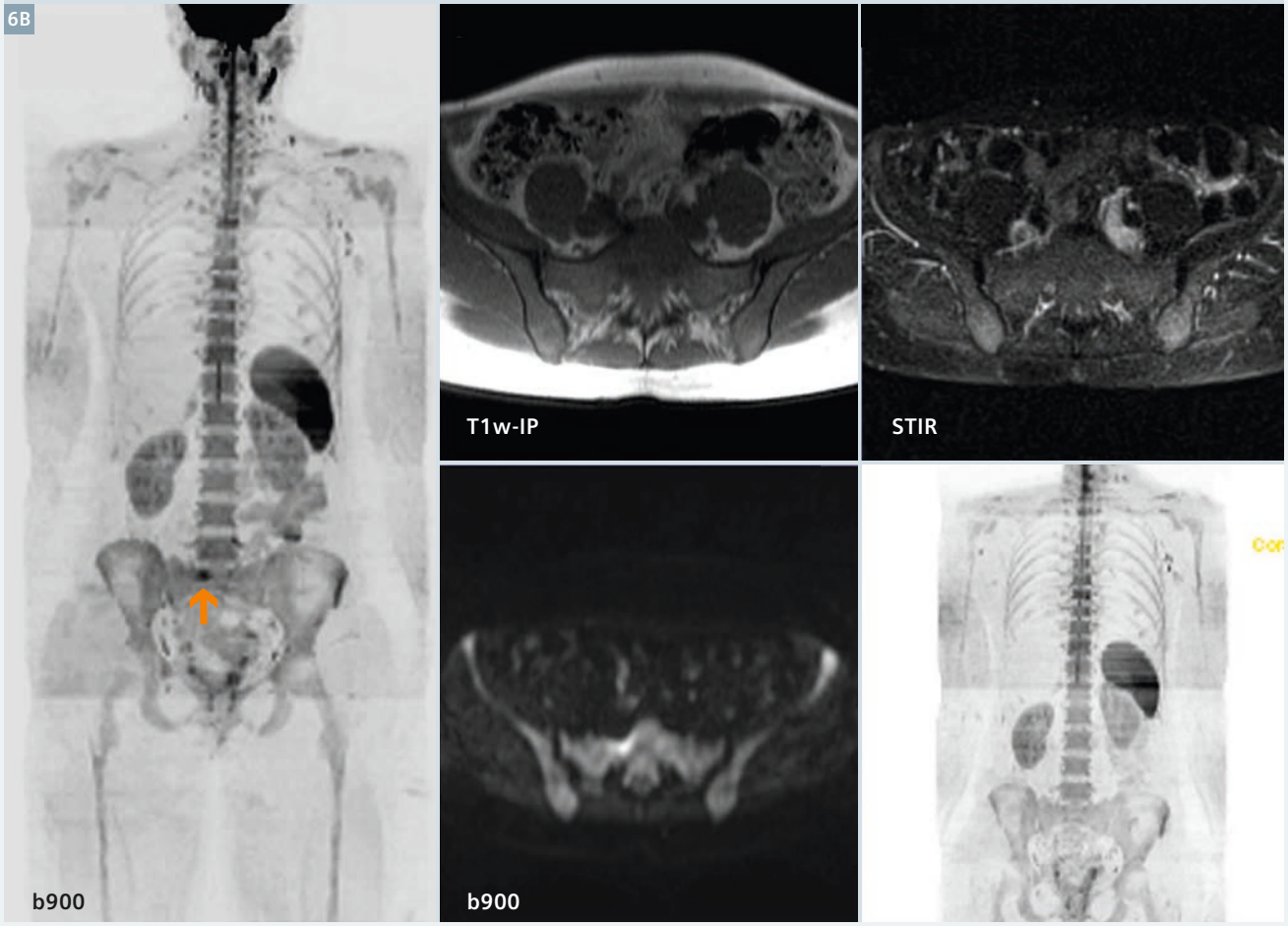

and in patients treated with hematopoietic growth factors such as granulocyte-colony stimulating factors (G-CSF).

Causes for false-positive findings include bone marrow edema caused by fractures, osteoarthritis, infection, bone infarcts, vertebral hemangiomas, isolated bone marrow islands and 'T2 shine through' – the latter observed in treated metastases. A variety of internal metallic (orthopedic) and silicone (breast) prostheses are routinely encountered in clinical practice. Magnetic field inhomogeneities secondary to metal and air interfaces will cause artifacts that cause false positive lesions (Fig. 6) and at the same time may obscure metastatic lesions in the adjacent bones. Many of these false-positive findings can be identified as not representing metastases by correlating the appearances of DW images with corresponding ADC maps and anatomical sequences [5].

Conclusions

WB-DWI is a contemporary imaging technique serving as an adjunct to conventional morphological whole body MRI, with high intrinsic sensitivity for detecting skeletal bone marrow metastases. However, there are several pitfalls that are encountered in routine clinical practice, the majority of which can be overcome by judicious interpretation of images in conjunction with standard anatomical sequences in light of relevant clinical knowledge.

References

1 Wu LM, Gu HY, Zheng J, et al. Diagnostic value of whole-body magnetic resonance imaging for bone metastases: a systematic review and meta-analysis. J Magn Reson Imaging 2011;34:128-135.
2 Padhani AR, Gogbashian A. Bony metastases: assessing response to therapy with whole-body diffusion MRI. Cancer Imaging 2011;11 Spec No A:S129-145.
3 Padhani AR. Diffusion magnetic resonance imaging in cancer patient management. Semin Radiat Oncol 2011;21:119-140.
4 Koh DM, Blackledge M, Padhani AR, et al. Whole-Body Diffusion-Weighted MRI: Tips, Tricks, and Pitfalls. AJR Am J Roentgenol 2012;199:252-262.
5 Padhani AR, Koh DM, Collins DJ. Whole-body diffusion-weighted MR imaging in cancer: current status and research directions. Radiology 2011;261:700-718.
6 Hwang S, Panicek DM. Magnetic resonance imaging of bone marrow in oncology, Part 1. Skeletal Radiol 2007;36:913-920.
7 Messiou C, Collins DJ, Morgan VA, Desouza NM. Optimising diffusion weighted MRI for imaging metastatic and myeloma bone disease and assessing reproducibility. Eur Radiol 2011;21:1713-1718.
8 Hillengass J, Bauerle T, Bartl R, et al. Diffusion-weighted imaging for non-invasive and quantitative monitoring of bone marrow infiltration in patients with monoclonal plasma cell disease: a comparative study with histology. Br J Haematol 2011;153:721-728.
9 Nonomura Y, Yasumoto M, Yoshimura R, et al. Relationship between bone marrow cellularity and apparent diffusion coefficient. J Magn Reson Imaging 2001;13:757-760.
10 Eiber M, Holzapfel K, Ganter C, et al. Whole-body MRI including diffusion-weighted imaging (DWI) for patients with recurring prostate cancer: Technical feasibility and assessment of lesion conspicuity in DWI. J Magn Reson Imaging 2011;33:1160-1170.

Contact

Professor Anwar R. Padhani, MB BS, FRCP, FRCR
Paul Strickland Scanner Centre
Mount Vernon Cancer Centre
Rickmansworth Road
Northwood
Middlesex HA6 2RN
United Kingdom
Phone: +44 (0) 1923-844751
Fax: +44 (0) 1923-844600
anwar.padhani
@stricklandscanner.org.uk